

PAPER

Study the structure of the low-lying states of ²⁰⁶Po

To cite this article: D Kocheva et al 2024 Phys. Scr. 99 065307

View the <u>article online</u> for updates and enhancements.

You may also like

- Systematic study of decay half-lives within the Generalized Liquid Drop Model with various versions of proximity energies Jun-Gang Deng, , Hong-Fei Zhang et al.
- Two-delta shell resonance description of decay: analytic expression of half-life via energy derivative of phase-shift Basudeb Sahu
- Simulation of the fission dynamics of the excited compound nuclei ²⁰⁶Po and ¹⁶⁸Yb produced in the reactions ¹²C+¹⁹⁴Pt and ¹⁸O+¹⁵⁰Sm
- H. Eslamizadeh and F. Bagheri

Physica Scripta



RECEIVED

31 January 2024

REVISED 12 April 2024

ACCEPTED FOR PUBLICATION 29 April 2024

PUBLISHED 16 May 2024 **PAPER**

Study the structure of the low-lying states of ²⁰⁶Po

D Kocheva¹, G Rainovski¹, J Jolie², M Beckers², A Blazhev², A Esmaylzadeh², C Fransen², K A Gladnishki¹, N Pietralla³, M Scheck⁴, F Spee², M Stoyanova¹, V Werner³, G De Gregorio^{5,6}, A Gargano⁶ and B Alex Brown⁷

- ¹ Faculty of Physics, St. Kliment Ohridski University of Sofia, 1164 Sofia, Bulgaria
- ² Institut für Kernphysik, Universität zu Köln, 50937 Cologne, Germany
- Institut f
 ür Kernphysik, Technische Universit
 ät Darmstadt, 64289 Darmstadt, Germany
- ⁴ CEPS, University of the West of Scotland, Paisley PA1 2BE, United Kingdom
- ⁵ Dipartimento di Matematica e Fisica, Università degli Studi della Campania Luigi Vanvitelli, I-81100 Caserta, Italy
- ⁶ INFN Sezione di Napoli, IT-80126 Napoli, Italy
- Michigan State University, East Lansing, MI 48824-1321, United States of America

E-mail: dkocheva@phys.uni-sofia.bg

Keywords: experimental nuclear physics, lifetime measurements, transfer reaction, single-particle excitations, collective excitations

Abstract

The nucleus 206 Po was studied in the two proton transfer reaction 204 Pb(16 O, 14 C) 206 Po and the lifetime of the first excited 2^+ state was determined by utilizing the Recoil Distance Doppler Shift method. The experimental results are compared with shell-model calculations based on different effective interactions. The calculations qualitatively reproduced the experimentally observed $B(E2; 2_1^+ \rightarrow 0_1^+)$ value, suggesting that the 2_1^+ state of 206 Po exhibits a collective nature. However, the employed effective interactions revealed some limitations, particularly in their description of the $4_{1,2}^+$ states. These results emphasize the importance of understanding the properties of low-lying states, especially their evolution from single-particle dynamics to collective modes, in evaluating various effective nuclear interactions.

1. Introduction

The dynamics of the nuclear many-body system emerge from an intricate interplay single-particle motion of individual nucleons and their correlated, collective behavior. The description of single-particle motion within nuclei is well understood within the nuclear shell model [1]. Apart from the individual particle configuration, the nuclei are significantly influenced by pairing correlations. These correlations promote the formation of nucleon pairs with a coupled angular momentum of J=0. Then, in semi-magic nuclei, the low-energy yrast states are those with the fewest unpaired nucleons. This number of unpaired nucleons is called 'seniority' ν [2]. States with higher seniority appear at higher excitation energy. If seniority remains a good quantum number, then all states can be grouped into multiplets of one and the same seniority. The generalized seniority scheme [3, 4] is, in fact, a simplified version of the nuclear shell model. Within the generalized seniority scheme [3, 4], matrix elements remain unchanged between nuclei with n valence nucleons and those with valence nucleon numbers corresponding to the lowest seniority. Thus, the yrast spectra for even-n particle configurations mirror those found in a 2-particle configuration.

Unlike single-particle behavior, collective behavior in nuclei arises from the coherent motion of valence nucleons. This motion is driven by the residual proton-neutron interaction [5]. The way nuclear states evolve as the number of valence particles (or holes) increases (shifting from single-particle configurations to collective mixtures) is crucial for understanding the origins of nuclear collectivity and testing the accuracy of microscopic nuclear models.

A suitable region for such investigations is the region of Po isotopes nortwest of 208 Pb. In the last decade, the nuclei within this region have been subject to renewed scientic interest [6–10]. The energy spacing between the yrast 2^+ , 4^+ , 6^+ , and 8^+ states in 210 Po suggests a seniority-like structure. Excluding the $B(E2; 2_1^+ \rightarrow 0_1^+)$ value, the E2 transition strengths between these states align with the predictions of the seniority scheme [6]. In open-

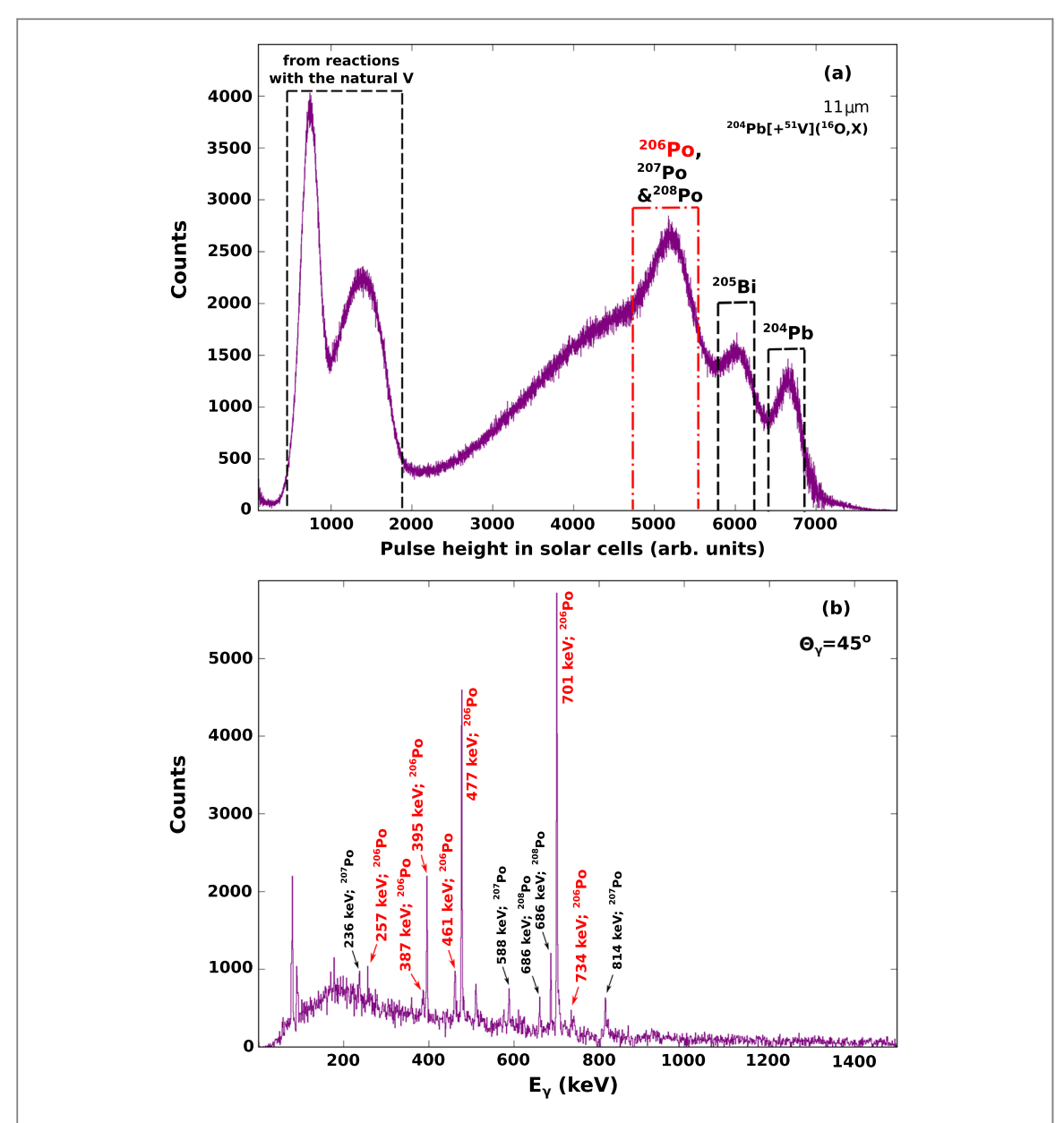


Figure 1. (a) The projection of the particle- γ matrix for the target-to-stopper distance $D=11~\mu m$ at $\Theta_{\gamma}=45^{\circ}$. Different parts of the particle spectrum are indicated in marked ranges and correspond to particles detected by the solar cells in coincidence mode with the γ rays from the labelled nuclei. (b) The particle-gated γ -ray spectrum which is obtained in coincidence with the region labelled as c206 Po, 207 Po & 208 Po' in panel (a).

shell polonium isotopes with N < 126, the transition from seniority configurations to collectivity as the number of neutron holes increases remains an unexplored area. The 2_1^+ state energy drops by 495 keV from 210 Po to 208 Po, suggesting increased collectivity after removing two neutrons from the N=126 shell. Yet, this energy stays almost a constant for isotopes down to 200 Po (N = 116), a behavior typical for seniority configurations (see figure 1 in [11]). In addition, the facts that the 6_1^+ and 8_1^+ states of $^{208-200}$ Po isotopes are closely spaced and that they have identical magnetic moments [12] strongly suggest that these states are seniority type excitations, built predominantly on the $\pi(h_{9/2})^2$ configuration, similar to those in ²¹⁰Po. Therefore, to understand the transition from seniority dominated to collective behaviour in open-shell polonium isotopes with N<126, it is important to analyze the evolution of the absolute E2 strengths. Taking away a neutron from ²¹⁰Po does not result in an increase in the quadrupole collectivity for the low-lying states of ²⁰⁹Po. This observation persists even for ²⁰⁸Po, which has two neutron holes with respect to 210 Po. In our previous study we concluded that the 4_1^+ states of 204,206 Po acquired collectivity due to the relatively enhancement of the $4_1^+ o 2_1^+$ transition with respect to expectations of simple mixture of proton and neutron seniority configuration [8]. However, the exact character of the 2_1^+ state of ²⁰⁶Po is still uncertain. Grahn *et al* have measured the $B(E2; 2_1^+ \to 0_1^+)$ value for ²⁰⁶Po using Coulomb excitation with re-accelerated radioactive beams in inverse kinematics [11]. The large uncertainty in the obtained transition strength, $B(E2; 2_1^+ \rightarrow 0_1^+) = 18_{-11}^{+14} \text{W.u.}$, makes it challenging to definitively interpret

the nature of the 2_1^+ state in 206 Po. This has motivated us to perform an experiment dedicated to measure the lifetime of the 2_1^+ state of 206 Po utilizing a different experimental technique. The results from this experiment are presented and discussed in the present study.

2. Experimental setup

The excited states of 206 Po were populated using the 204 Pb(16 O, 14 C) 206 Po—two protons transfer (2*p*-transfer) reaction. The 16 O beam of energy 84 MeV was provided by the FN-TANDEM accelerator at the University of Cologne. The mean lifetime of the 2_1^+ state of 206 Po was measured by utilizing the Recoil Distance Doppler Shift (RDDS) method [13, 14]. The target was a 0.6 mg cm $^{-2}$ thin 204 Pb layer with 99.94% isotopic enrichment evaporated on a 0.3 mg cm $^{-2}$ Support foil. The target was positioned so that the side of the vanadium foil was facing the beam. The stopper was a 2.0 mg cm $^{-2}$ Support foil and was stretched parallel to the target. Data were taken at six plunger distances: 11 μ m, 13 μ m, 17 μ m, 21 μ m, 30 μ m and 47 μ m. These distances were determined relative to the electrical contact of the foils obtained via the capacitance method [15, 16] and were kept constant by the active feedback system of the Cologne plunger device [15].

The target and the stopper were placed inside the chamber of the Cologne plunger device [15]. In order to detect the recoiling light reaction fragments, in the chamber was mounted an array of six (10 mm \times 10 mm) solar cells. They were positioned at backward angles with respect to the beam direction and covered an angular range between 115° and 165°. The solar cells serve for a selection of the different reactions induced on the target and the stopper. Due to the large mass difference of the target and backing and stopper materials the transfer reactions induced on the target and the backing and/or stopper are well separated (as can be seen in figure 1(a)). For detecting the γ rays from the decay of the excited states of ²⁰⁶Po was used an array of eleven high purity germanium (HPGe) detectors. The detectors were placed in two rings around the target chamber: five of them were placed at 142° and the other six of them were placed at 45°.

3. Data analysis and results

The data were sorted offline when at least one solar cell and one HPGe detector are in coincidence which corresponds to particle- γ coincidences and when at least two HPGe detectors are in coincidence which corresponds to γ - γ coincidences. As an example, in figure 1(a) is presented a projection of one of the sorted particle- γ matrices. This matrix is sorted for the data obtained at target-to-stopper distance 11 μ m and for germanium detectors placed at forward angles. Different parts of the projection of the particle- γ matrix are indicated in marked ranges and correspond to particles detected by the solar cells in coincidence mode with the γ rays coming from the labelled nuclei. The γ rays which are found to be in coincidence with the particles labelled components and its intensitions depopulating excited states of possible γ 00. Moreover, the transition depopulating the first excited γ 01 state of coincidence with the particle-gated γ 11 state of coincidence with the particle depend on the plunger distance, as can be seen in figure 2. In this figure are presented the particle-gated γ 1 ray spectra of the γ 1 transition at three different plunger distances observed at backward (a) and forward (b) angles. As can be expected, as the distance between the target and the stopper increases, the intensity of the shifted components increases as well.

Studying the change of the intensities of the shifted (I_{sh}) and the unshifted (I_{un}) components of the $2_1^+ \to 0_1^+ \gamma$ -ray transition enables the determination of the lifetime of the 2_1^+ state of ²⁰⁶Po. The data from the present experiment was analyzed by means of the Differential Decay Curve Method (DDCM) [17, 18]. This method requires the I_{sh} and I_{un} components (for each distance) to be measured from spectra which are in coincidence with Doppler-shifted components of transitions that are direct feeders of the state of interest. Then the lifetime τ_i for the i-th target-to-stopper distance can be determined via [17, 18]:

$$\tau_i(x) = \frac{I_{un}(x)}{\left\langle v \right\rangle \frac{d}{dx} I_{sh}(x)}.$$
 (1)

In our analysis the lifetime is determined by the software program Napatau [19]. The program fits the I_{sh} components and calculates over separate intervals the time derivative of that curve. Then the trend of the time-derivative is adapted to the trend of the I_{un} components.

As can be seen from equation (1) the velocity of the ejected 206 Po nuclei has to be known. In our analysis the mean velocity of the recoiling nuclei $\langle \nu \rangle$ was determined experimentally using the centroids' positions of the shifted and the unshifted components of the 701-keV transition to be $\langle \nu \rangle = 1.09(7)\%c$. In order to extract the lifetime of the state of interest in the present experiment, the data have to be analyzed in particle- γ - γ coincidence

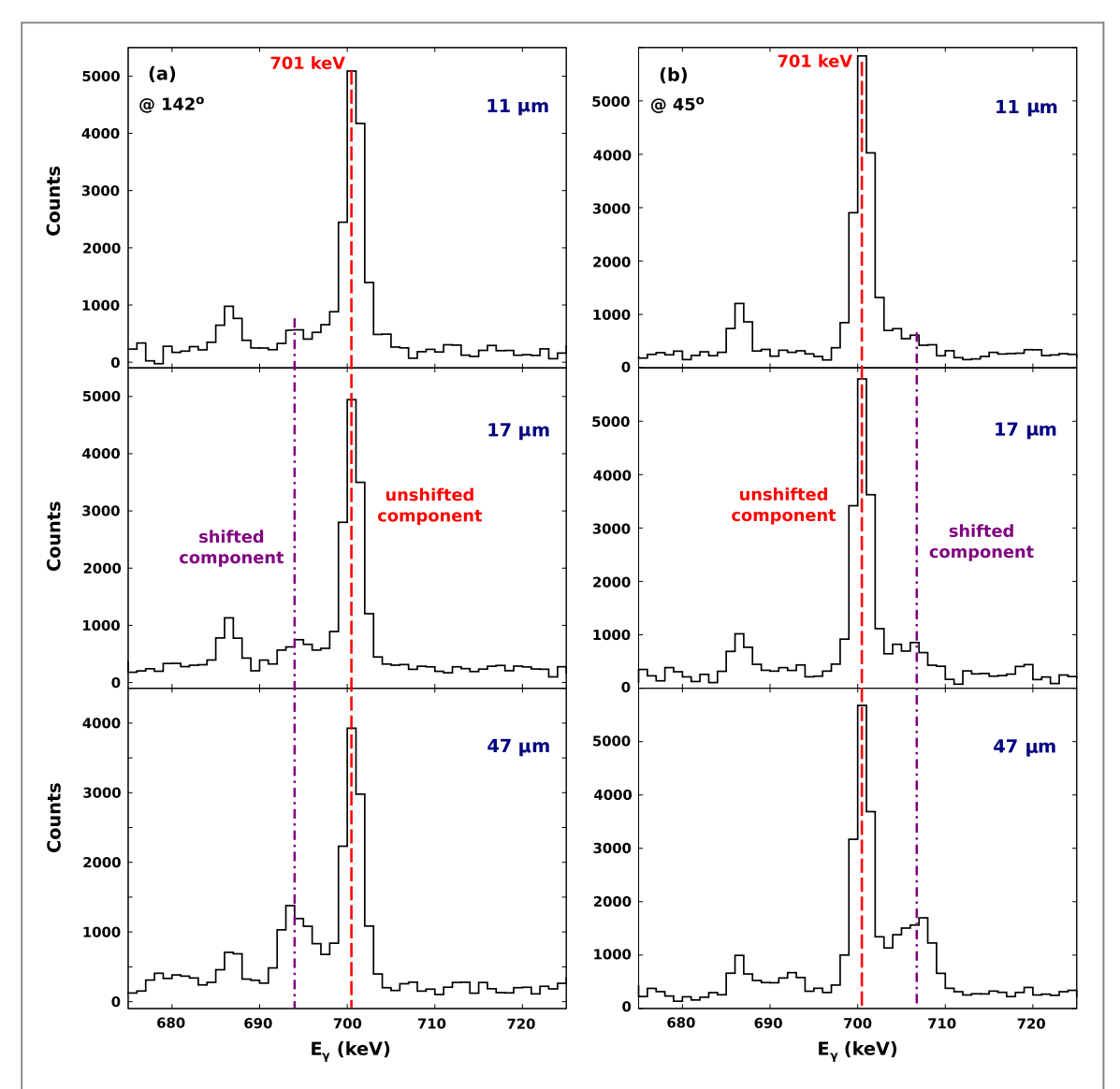


Figure 2. The evolution of the intensities of the unshifted and Doppler-shifted peak of the 701-keV $(2_1^+ \rightarrow 0_1^+)$ transition observed at backward angles (a) and at forward angles (b) for three different plunger distances. The dash-dotted (violet) lines represent the positions of the Doppler-shifted peak and the dashed (red) lines represent the unshifted peak positions.

mode. Due to the acquired level of statistics this requirement cannot be met. However, the particular feeding pattern of the first 2^+ state of 206 Po allows circumvention of this problem, as described below.

The presented particle-gated spectra (figure 1(b) and figure 2) are, in fact, singles spectra. In principal, the singles γ -ray spectra contain information for the effective lifetime which aggregates the mean lifetime of the state of interest and the partial lifetimes of all states decaying to it. Hence, the intensities of the 701-keV line that are derived from the spectra in figure 2 have to be corrected for the effects of the transitions that feed directly the state of interest. Due to the specific mechanism of the transfer reactions, they only populate discrete states which is in contrast to fusion-evaporation reactions. Therefore, it can be considered that in the present analysis slow feeding contributions to the effective lifetimes of excited states of ²⁰⁶Po can originate only from discrete decays of higher-lying states, as suggested in [20]. A partial level scheme of the states of ²⁰⁶Po populated via the used 2*p*-transfer reaction was constructed on the basis of the particle- γ and γ - γ coincidences. The resulting level scheme from the present data is shown in figure 3. It agrees with the previously reported level schemes of ²⁰⁶Po [21]. For the spin-parities of the observed states, we have adopted the values reported in previous studies [21]. It is important to emphasize that besides the levels depicted in figure 3 there are no other states observed up to date that decay directly to the 2_1^+ state of ²⁰⁶Po. This means that there are four direct feeders to the level of interest whose effects have to be accounted.

The lifetimes of the 4_2^+ and 2_2^+ states at excitation energies 1434 keV and 1162 keV, respectively, are not known. In the present data the 734-keV ($4_2^+ \rightarrow 2_1^+$) and 461-keV ($2_2^+ \rightarrow 2_1^+$) transitions have Doppler-shifted and stopped (unshifted) components. Hence, the contributions coming from the decays of both states to the 2_1^+ state could not be considered neither as fast nor as slow feeding. Therefore, to determine accurately the intensity

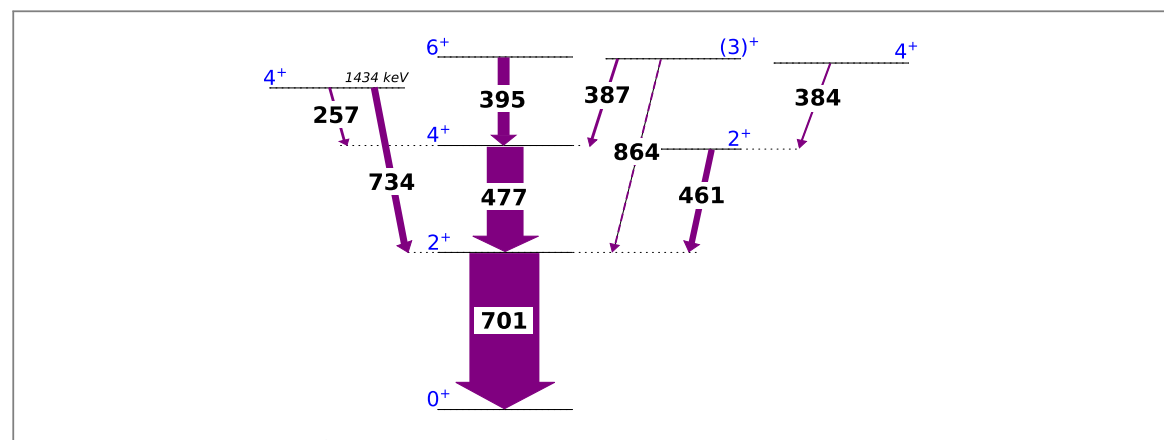


Figure 3. Partial level scheme of 206 Po obtained with the 2p-transfer reaction in the present work. The arrows' thicknesses are proportional to the relative γ -ray intensities normalized to the intensity of the 701-keV $(2_1^+ \to 0_1^+)$ transition. The 864-keV transition (dashed line) is not observed in the present RDDS data but the 387-keV line is observed.

of the unshifted component of the 701-keV line, we have taken into account the additional counts from the $4_2^+ \rightarrow 2_1^+$ and $2_2^+ \rightarrow 2_1^+$ decays when the nucleus is at rest. This means that we have subtracted the I_{un} components of the 734-keV and 461-keV lines from the I_{un} component of the 701-keV line. The intensities of the lines were efficiency-corrected before this procedure. In addition to the main analysis, we have estimated also the lifetime of the 4_2^+ state of 2^{206} Po to be 7(3) ps in an analogous way as for the 2_1^+ state. This lifetime corresponds to transition strength of $B(E2; 4_2^+ \rightarrow 2_1^+) = 540(231) \, \mathrm{e}^2 \mathrm{fm}^4$.

The lifetime of the 4_1^+ state of 206 Po has been measured by γ - γ fast timing technique to be 89(7) ps [8]. In the present data Doppler-shifted component of the 477-keV ($4_1^+ \rightarrow 2_1^+$) transition appears at the longer plunger distances. Therefore, we corrected the intensity of the stopped component of 701-keV line with the intensity of the stopped component of 477-keV transition analogous to the 734-keV and 461-keV feeder transitions.

Then only the 864-keV $((3_1)^+ \rightarrow 2_1^+)$ transition has not been taken into account. Due to the low statistic in the present RDDS experiment the 864-keV line is not visible but the 387-keV transition depopulating the same excited level is observed (see figure 1(b)). This line is contaminated by the 384-keV $(4_3^+ \to 2_2^+)$ transition. In our data not only the stopped components of both lines are observed but also some Doppler shifted components. Due to the lack of information about the lifetimes of the $(3_1)^+$ and 4_3^+ states and the close energies of both transitions we cannot separate certainly the counts of the 387-keV line from the counts of the 384-keV line. During the experiment beside the present RDDS measurements we have performed an additional measurement which has utilized the same transfer reaction on a 25 mg cm $^{-2}$ -thick foil of 204 Pb as target. The experimental setup and the beam energy are the same as in our RDDS experiment and therefore, similar relative population of the excited states of 206 Po can be expected. Indeed, the data from the additional measurement show that 54(1)%from the feeding of the 2_1^+ state is coming from the $4_1^+ \rightarrow 2_1^+$ transition. This result is in agreement with the data from the present RDDS experiment where this feeding is determined to be 53(4)%. The intensities of the other direct feeders of the 2_1^+ state of 206 Po observed from the additional data show that 9.5(7)% from the feeding of the 2₁⁺ state originates from the 734-keV transition, 9(1)% is coming from 461-keV transition and 2.7(5)% originates from the 864-keV transition. The remaining 24.8% of the intensity of the 701-keV transition is considered as direct population of the 2_1^+ state. Since the $(3_1)^+$ state could not be considered neither as fast nor as slow feeder we have assumed these two limits and we accounted for their influence in our analysis in a similar way as in our previous studies [9, 22]. Firstly, if we assume that its lifetime is short enough so that it decays only in flight, no further corrections of the intensities of the 701-keV transition are needed. Therefore, the intensities of both components of the 701-keV transition that are determined with the above-mentioned procedure can be used to determine the lifetime of the 2_1^+ state of 206 Po using the equation (1). The DDCM analysis for the lifetime of the state of interest is presented in figure 4 for backward (a) and forward (b) angles. The average value between both results gives the value of 6.4(7) ps for the lifetime of the 2_1^+ state of 206 Po. Considering the alternative for the lifetime of the $(3_1)^+$ state, namely that it is long-lived and decays only at rest, we have further reduced the stopped component of the 701-keV line by 2.7% of the total intensity. Then the lifetime of the 2_1^+ is reduced to 5.9(6) ps. By averaging the two limits we obtained the value of 6.2 ps with a statistical uncertainty of 0.5 ps and an additional systematic uncertainty of 0.9 ps. As the final value for the lifetime of the 2_1^+ we adopted the value of 6.2 (10) ps. Using this lifetime and the electron conversion coefficient for the $2_1^+ \rightarrow 0_1^+$ transition of 206 Po [21] we have calculated that the absolute transition strength is $B(E2; 2_1^+ \rightarrow 0_1^+) = 766(124) e^2 \text{fm}^4 = 10.6(17) \text{ W.u.}$

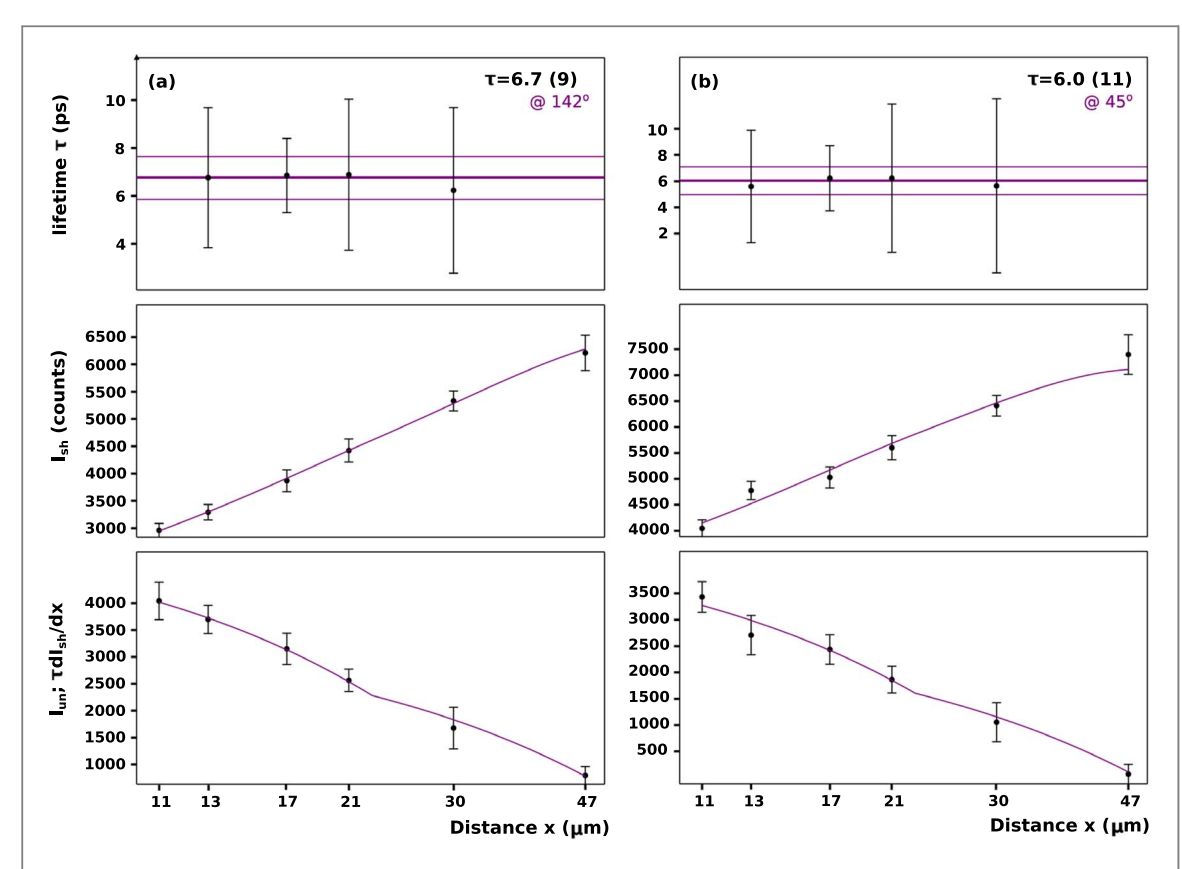


Figure 4. The lifetime of the 2_1^+ state of 206 Po determined at backward (a) and forward angles (b). The graphs in the middle panels illustrate the shifted intensities at various target-to-stopper distances. To calculate the derivative, continuous curves are fitted through these intensities. The bottom panels compare the curves that represent the product between the lifetime of the state of interest and the time derivatives of the shifted intensities with the experimental unshifted intensities. The upper panel shows the extracted lifetimes for each distance in the region of sensitivity. The weighted mean values of the lifetimes are indicated by the horizontal lines.

4. Discussion

In the present study the structure of the first excited nuclear state of ²⁰⁶Po has been investigated in the framework of the shell model using the code KSHELL [23]. For the purpose of these calculations, the double-magic nucleus 208 Pb has been considered as a closed inert core. The calculations are performed in a similar way as in our previous studies of ^{208,209}Po [7, 9]. For both proton particles and neutron holes the model space included the orbitals $2p_{3/2}$, $2p_{1/2}$, $1f_{7/2}$, $1f_{5/2}$, $0h_{9/2}$, $0i_{13/2}$. As in our studies [7, 9], the \hat{Q} -box folded-diagram approach [24] was used for the two-body matrix elements of the effective Hamiltonian. The starting point here is the CD-Bonn nucleon-nucleon potential [25] renormalized utilizing the $V_{\rm low-k}$ approach [26] (henceforth these calculations will be labelled as CD-Bonn calculations). The Coulomb potential is also included for the proton-proton interaction. The proton single-particle and neutron single-hole components of the effective Hamiltonian have been taken from the experimental spectra of ²⁰⁹Bi [27] and ²⁰⁷Pb [28], respectively. The effective charges used in the present study are $e_{\pi} = 1.5e$ and $e_{\nu} = 0.92e$ and are the same as in [7].

A comparison between the experimental and calculated spectra of ²⁰⁶Po is shown in figure 5. The calculated excitation energies of the yrast states are in a very good agreement with the experimental data, as the discrepancies are less than 80 keV for all of the states. The comparison of the B(E2) transition strengths shows very good agreement for the $8_1^+ \to 6_1^+$ transition, and good agreement in the case of the $2_1^+ \to 0_1^+$ transition. Both the newly derived experimental $B_{exp}(E2; 2_1^+ \rightarrow 0_1^+) = 766(124) e^2 \text{fm}^4$ value and the calculated one $B_{th}(E2; 2_1^+ \rightarrow 0_1^+) = 541 \text{ e}^2 \text{fm}^4 \text{ show significant increase compared with the ones in the case of }^{208} \text{Po}$ $B_{exp}(E2; 2_1^+ \to 0_1^+) = 252(96) \text{ e}^2 \text{fm}^4 \text{ and } B_{th}(E2; 2_1^+ \to 0_1^+) = 388 \text{ e}^2 \text{fm}^4 \text{ [9]}.$ This allows us to conclude that the increase of the neutron holes in N = 126 shell closure increases the collectivity of the 2_1^+ states. However, the CD-Bonn calculations cannot describe the $B(E2; 6_1^+ \to 4_1^+)$ and $B(E2; 4_{1,2}^+ \to 2_1^+)$ values. To discuss further the structure of the low-lying states of 206 Po, their wave functions are presented in terms

of the $|^{204}\text{Pb}\rangle \otimes |^{210}\text{Po}\rangle$ basis states:

$$|^{206} \text{ Po; } 0_{\text{gs}}^{+}\rangle = 0.98|^{204} \text{Pb; } 0_{\text{gs}}^{+}\rangle \otimes |^{210} \text{Po; } 0_{\text{gs}}^{+}\rangle + \dots$$
 (2)

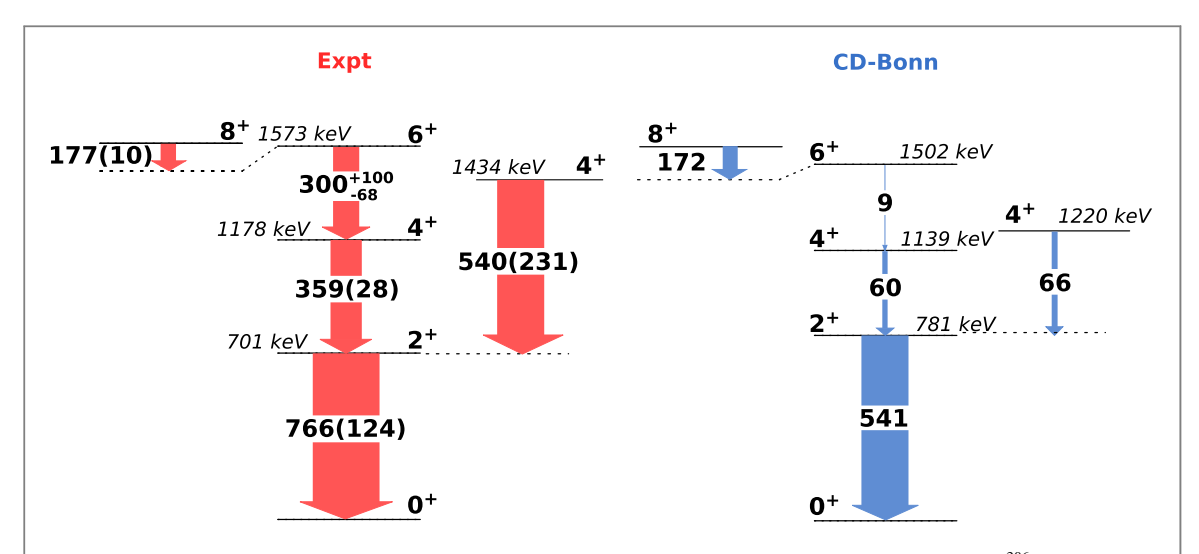


Figure 5. A graphical representation of the results for shell-model calculations (CD-Bonn) for the low-lying states in 206 Po in comparison with experimental data (Expt). The experimental $B(E2; 8_1^+ \to 6_1^+)$ value is taken from [21], the $B(E2; 6_1^+ \to 4_1^+)$ value is taken from [29], the $B(E2; 4_1^+ \to 2_1^+)$ value is taken from [8] and the other results are from the present study. The thickness of the arrows is proportional to the B(E2) values in e^2 fm⁴. The latter are also presented by the numbers next to the arrows.

Table 1. Comparison between the experimental and calculated (CD-Bonn) properties of the low-lying states in ²⁰⁴Pb. The experimental *B* (*E*2) values are from [30].

J_i^π	$E_x(\text{MeV})$		J_f^π	$B(E2; J_i \rightarrow J_f)(e^2 \text{ fm}^4)$	
	Expt	CD-Bonn	,,	Expt	CD-Bonn
21+	0.899	0.840	0_{1}^{+}	334(4)	295
4_1^+	1.274	1.178	2_{1}^{+}	0.27(1)	65
4_2^+	1.563	1.275	2_{1}^{+}	_	10

$$|^{206} \text{ Po; } 2_1^+\rangle = 0.93|^{204} \text{Pb; } 2_1^+\rangle \otimes |^{210} \text{Po; } 0_{gs}^+\rangle -0.30|^{204} \text{Pb; } 0_{gs}^+\rangle \otimes |^{210} \text{Po; } 2_1^+\rangle + \dots$$
 (3)

$$|^{206} Po; \ 4_1^+\rangle = -0.96 |^{204} Pb; \ 4_1^+\rangle \otimes |^{210} Po; \ 0_{gs}^+\rangle + 0.14 |^{204} Pb; \ 4_2^+\rangle \otimes |^{210} \ Po; \ 0_{gs}^+\rangle - 0.14 |^{204} Pb; \ 0_{gs}^+\rangle \otimes |^{210} Po; \ 4_1^+\rangle + ... \eqno(4)$$

$$|^{206} \text{ Po; } 6_1^+\rangle = -0.96|^{204} \text{Pb; } 0_{gs}^+\rangle \otimes |^{210} \text{Po; } 6_1^+\rangle -0.17|^{204} \text{Pb; } 2_1^+\rangle \otimes |^{210} \text{Po; } 4_1^+\rangle + \dots$$
 (5)

$$|^{206} \text{ Po; } 8_1^+\rangle = -0.96|^{204} \text{Pb; } 0_{gs}^+\rangle \otimes |^{210} \text{Po; } 8_1^+\rangle - 0.22|^{204} \text{Pb; } 2_1^+\rangle \otimes |^{210} \text{Po; } 8_1^+\rangle + \dots$$
 (6)

$$|^{206}\text{Po; } 4_{2}^{+}\rangle = 0.14|^{204}\text{Pb; } 4_{1}^{+}\rangle \otimes |^{210}\text{Po; } 0_{gs}^{+}\rangle + 0.94|^{204}\text{Pb; } 4_{2}^{+}\rangle \otimes |^{210}\text{ Po; } 0_{gs}^{+}\rangle -0.17|^{204}\text{Pb; } 0_{es}^{+}\rangle \otimes |^{210}\text{Po; } 4_{1}^{+}\rangle$$
(7)

The wave functions of the 2_1^+ and 4_1^+ states are neutron dominated while the 6_1^+ and 8_1^+ states are dominated by the proton components. A more detailed discussion deserve the 4_1^+ and 4_2^+ states whose wave functions are predicted to contain 92% from the 4_1^+ state of 204 Pb and 88% from the 4_2^+ state of 204 Pb, respectively (see equations (4) and (7)). This neutron dominance in the structures of the $4_{1,2}^+$ states can be the reason for the observed discrepancy between the theoretical and the experimental $B(E2; 4_{1,2}^+ \to 2_1^+)$ values. In order to examine the origin of this issue we have performed calculations for 204 Pb using the same shell-model framework. The results are presented in table 1. It has to be noticed that the first and second 4^+ states in 204 Pb are predicted to lie, respectively, ≈ 100 and 300 keV below the experimental ones. These significant deviations are the reason for the overestimation of the neutron contribution in the structure of the first two 4^+ states of 206 Po which consequently lead to the small E2 transition strengths in the shell-model calculations indicating deficiencies in the n-n part of the used interaction.

It is interesting to check whether the problem is specific for the used interaction. For this purpose, we have performed another large-scale shell-model calculations with the KHM3Y effective interaction [31] (henceforth labelled as KHM3Y calculations). This interaction was developed for the Z=50-126 and N=82-184 model space. In order to make the calculations possible, the proton orbitals below the Z=82 were considered

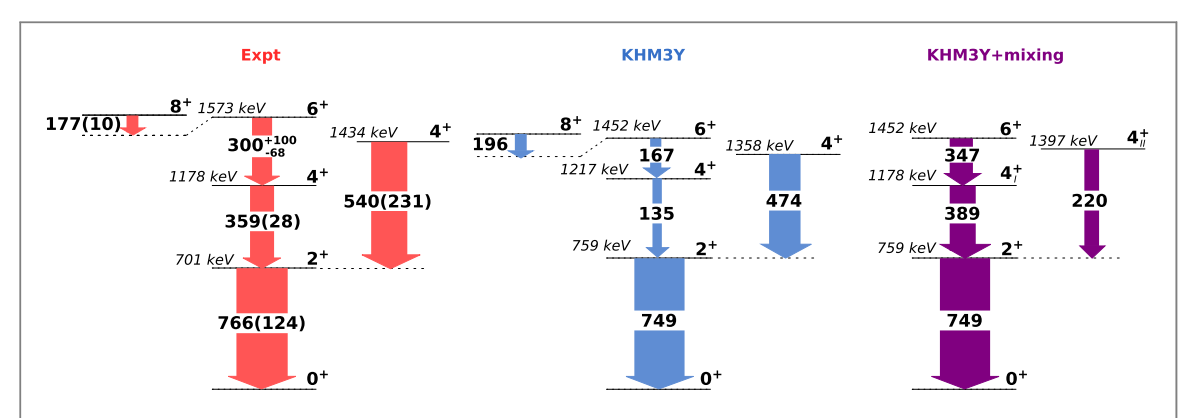


Figure 6. A graphical representation of the results for shell-model calculations with the KHM3Y interaction for the low-lying states in 206 Po in comparison with experimental data (Expt). The thickness of the arrows is proportional to the B(E2) values in e^2 fm⁴. The latter are also presented by the numbers next to the arrows (see text for details).

Table 2. Comparison between the experimental and calculated magnetic (μ) and quadrupole (Q) moments of $^{210-206}$ Po isotopes. The experimetal data is taken from [12].

	$\mu(\mu_N)$		Q(efm²)	
	Expt	КНМЗҮ	Expt	КНМЗҮ
²¹⁰ Po				
8_{1}^{+}	+7.13(5)	+7.31	-55(2)	-56
6_{1}^{+}	5.48(5)	+5.49	_	-12
²⁰⁸ Po				
8_{1}^{+}	+7.37(5)	+7.29	90(4)	-86
6_{1}^{+}	+5.3(6)	+5.39	_	-9
²⁰⁶ Po				
8_{1}^{+}	+7.34(7)	+7.22	102(4)	-91
6_1^+	_	+5.34	_	-16

completely filled and the neutron excitations across the N=126 shell were not allowed, hence, the same model space as in our previous calculations is used. The calculations were performed using the shell-model code NuShellX [32]. The effective neutron charge $e_{\nu}=1e$ is chosen to reproduce the $B(E2; 4_1^+ \rightarrow 2_1^+)$ and $B(E2; 2_1^+ \rightarrow 0_1^+)$ values in 204,206 Pb, and the $e_{\pi}=1.6e$ is chosen to reproduce the $B(E2; 8_1^+ \rightarrow 6_1^+)$ transition strength in 210 Po. For effective gyromagnetic factors, we adopted the values recommended in [33]: $g_{\pi}^s=3.234$, $g_{\nu}^s=-2.083$, $g_{\pi}^l=1.107$, and $g_{\nu}^l=-0.065$. The radial part of the wave functions is calculated using the Skyrme potential [34]. It is worth mentioning that, with that choice of the effective multipole operators, the calculations reproduce very well the available experimental data on magnetic and quadrupole moments of the 8_1^+ and 6_1^+ states of all $^{210-206}$ Po isotopes as can be seen in table 2. The results from the calculations for the energies of the low-lying states of 206 Po and the transitions strengths are presented and compared with the experimental data in figure 6.

The calculated excitation energies of the yrast states are in a good agreement with the experimental ones as the discrepancies are less than 120 keV for all of the states. The comparison between the theoretical and experimental B(E2) values shows very good agreement of the $B(E2; 2_1^+ \to 0_1^+)$ transition strength and some improvements in the $B(E2; 6_1^+ \to 4_1^+)$ and $B(E2; 4_1^+ \to 2_1^+)$ values with respect to the CD-Bonn calculations. In order to obtain the wave functions of the calculated states in terms of the $|^{204}\text{Pb}\rangle \otimes |^{210}\text{Po}\rangle$ basis states, we have converted the KHMY3 interaction used in the NuShellX code [32] into the format for the KSHELL code [23] for the model space used. We have rigorously verified that both codes produce identical results for the energies of the excited states and the electromagnetic properties of $^{210-206}\text{Po}$ isotopes. The results from this procedure for the wave functions of the calculated states of ^{206}Po are presented as follow:

$$|^{206} \text{ Po; } 0^+_{gs}\rangle = 0.94|^{204} \text{Pb; } 0^+_{gs}\rangle \otimes |^{210} \text{Po; } 0^+_{gs}\rangle + ... \tag{8}$$

$$|^{206} \text{ Po; } 2_{1}^{+}\rangle = -0.77|^{204} \text{Pb; } 2_{1}^{+}\rangle \otimes |^{210} \text{Po; } 0_{gs}^{+}\rangle - 0.54|^{204} \text{Pb ; } 0_{gs}^{+}\rangle \otimes |^{210} \text{Po ; } 2_{1}^{+}\rangle + ...$$
 (9)

Table 3. Comparison between the experimental and calculated (KHM3Y) properties of the low-lying states in 204 Pb. The experimental B(E2) values are from [30].

J_i^{π}	$E_x(\mathrm{MeV})$		J_f^π	$B(E2; J_i \rightarrow J_f)(e^2 \text{ fm}^4)$	
	Expt	KHM3Y	,,	Expt	КНМ3Ү
2+	0.899	0.927	0_1^+	334(4)	328
4_1^+	1.274	1.317	2_{1}^{+}	0.27(1)	9
4_2^+	1.563	1.593	2_{1}^{+}	_	205

$$|^{206}\text{Po; } 4_{1}^{+}\rangle = 0.75|^{204}\text{Pb; } 4_{1}^{+}\rangle \otimes |^{210}\text{Po; } 0_{gs}^{+}\rangle + 0.20|^{204}\text{Pb; } 4_{2}^{+}\rangle \otimes |^{210}\text{ Po; } 0_{gs}^{+}\rangle -0.46|^{204}\text{Pb; } 0_{gs}^{+}\rangle \otimes |^{210}\text{Po; } 4_{1}^{+}\rangle + \dots$$
(10)

$$|^{206} \text{ Po; } 6_1^+\rangle = 0.91|^{204} \text{Pb; } 0_{\text{ss}}^+\rangle \otimes |^{210} \text{Po; } 6_1^+\rangle + \dots$$
 (11)

$$|^{206} \text{ Po; } 8_1^+\rangle = -0.89|^{204} \text{Pb; } 0_{gs}^+\rangle \otimes |^{210} \text{Po; } 8_1^+\rangle + \dots$$
 (12)

$$|^{206}Po;\ 4_{2}^{+}\rangle = 0.53|^{204}Pb;\ 4_{1}^{+}\rangle \otimes |^{210}Po;\ 0_{gs}^{+}\rangle - 0.26|^{204}Pb;\ 4_{2}^{+}\rangle \otimes |^{210}\ Po;\ 0_{gs}^{+}\rangle + 0.61|^{204}Pb\ ;\ 0_{gs}^{+}\rangle \otimes |^{210}Po;\ 4_{1}^{+}\rangle \quad (13)$$

Similarly to the CD-Bonn calculations, KHM3Y calculations also predict that the 6_1^+ and 8_1^+ states are dominated by the proton components. Although the 2_1^+ and $4_{1,2}^+$ states are still predicted to be dominated by the neutron components, the contributions of the proton components increase significantly expecially in the case of the 4_2^+ state. This improvement can be traced to the n-n part of the KHM3Y interactions by calculating the properties of the excited states of 204 Pb in the same shell-model framework. These results are presented in table 3. The energies of the 2_1^+ , 4_1^+ and 4_2^+ excited states of 204 Pb are well reproduced. In addition the calculated E2 transition strengths agree well with the available experimental values especially for the decay of the 4_1^+ state of 204 Pb. Hence, the problem existing in the n-n part of the CD-Bonn interaction does not appear in the KHM3Y interaction.

Regardless of the improvement in the structures of the calculated $4_{1,2}^+$ states, the discrepancies between the experimental and the calculated $B(E2; 4_1^+ \to 2_1^+)$ and $B(E2; 6_1^+ \to 4_1^+)$ values are still significant (see figure 6). It has to be noted however that the excitation energies of the calculated $4_{1,2}^+$ states fall between those of the experimental $4_{1,2}^+$ states, as depicted in figure 6. This implies that introducing additional mixing to the calculated states could improve the description. Indeed, by introducing a mixing interaction of just 84 keV, the energy of the calculated 4_1^+ state can be aligned with the experimental 4_1^+ state's energy of 1178keV. In figure 6, the results of this mixing scenario are labelled as 'KHM3Y+mixing'. The states 4_I^+ and 4_{II}^+ result from the mixing of the calculated 4_1^+ and 4_2^+ states. The mixing elevates the energy of the 4_{II}^+ state to 1397keV and incorporates 18% of the structure of the calculated 4_2^+ state into the 4_I^+ state. The latter leads to $B(E2; 4_I^+ \to 2_I^+) = 389 \, \mathrm{e}^2 \, \mathrm{fm}^4$ and $B(E2; 4_{II}^+ \to 2_1^+) = 220 \, \mathrm{e}^2 \, \mathrm{fm}^4$. The $B(E2; 4_I^+ \to 2_1^+)$ value is in very good agreement with the experimental $B(E2; 4_I^+ \to 2_1^+) = 359(28) \, \mathrm{e}^2 \, \mathrm{fm}^4$ one. Moreover, the calculated $B(E2; 6_1^+ \to 4_I^+) = 347 \, \mathrm{e}^2 \, \mathrm{fm}^4$ is in agreement with the experimental $B(E2; 4_1^+ \to 2_1^+) = 300 \, \frac{100}{-600} \, \mathrm{e}^2 \, \mathrm{fm}^4$ value while the $B(E2; 4_{II}^+ \to 2_1^+)$ value is comparable with the experimental $B(E2; 4_2^+ \to 2_1^+)$ one. The necessity of introducing an additional mixing between the calculated $4_{1,2}^+$ states is an indication for minor deficiencies in KHM3Y most likely related to the p-n part of the interaction.

5. Summary

In the present study the lifetime of the 2_1^+ state of 206 Po was measured by the RDDS method. The determined $B(E2;\ 2_1^+\to 0_1^+)=10.6(17)$ W.u. value shows that the structure of this state is of collective nature. The experimental data was compared with shell-model calculations based on CD-Bonn and KHM3Y interactions. Both models describe well the properties of the 2_1^+ , 6_1^+ and 8_1^+ states confirming the collective nature of the 2_1^+ state and the single-particle, seniority-like, nature of the 6_1^+ and 8_1^+ ones. Both models have certain difficult in describing the properties of the 4_1^+ state. While in the case of CD-Bonn interaction these difficulties can be traced to some deficiencies in the n-n part of the interaction, KHM3Y interaction requires a small mixing between the calculated 4_1^+ and 4_2^+ states. The results from both calculations clearly show the spin-dependent character of the evolution from single-particle to collective behaviour and demonstrate the ability of the shell model to describe it. The present study also demonstrates that the low-lying states of nuclei transitioning from single-particle to collective mode exhibit marked sensitivity to minor components of the nucleon-nucleon interactions utilized in shell-model calculations.

Acknowledgments

This study is financed by the European Union-NextGenerationEU, through the National Recovery and Resilience Plan of the Republic of Bulgaria, project No BG-RRP-2.004-0008-C01. This work was supported by DAAD under the partnership agreement between the University of Cologne and University of Sofia and by the Bulgarian Ministry of Education and Science, within the National Roadmap for Research Infrastructures (object CERN). The authors acknowledge the Deutsche Forschungs Gemeinschaft (DFG) for the upgrade of the used germanium detectors under grant INST 216/988-1 FUGG. The members of the UWS Nuclear Physics Research Group acknowledge financial support from the UK Science and Technology Facilities Council (STFC, Grant No. ST/P005101/1). The study was supported by NSF grant PHY-2110365.

Data availability statement

All data that support the findings of this study are included within the article (and any supplementary files).

ORCID iDs

```
D Kocheva https://orcid.org/0000-0002-9068-4826
M Beckers https://orcid.org/0000-0002-7534-7282
A Blazhev https://orcid.org/0000-0003-1776-8510
K A Gladnishki https://orcid.org/0000-0001-8334-0059
M Scheck https://orcid.org/0000-0002-9624-3909
M Stoyanova https://orcid.org/0000-0002-0849-2359
G De Gregorio https://orcid.org/0000-0003-0253-915X
```

References

```
[1] Mayer M G 1950 Phys. Rev. 78 16
  [2] Racah G 1943 Phys. Rev. 63 367
  [3] Talmi I 1971 Nucl. Phys. A 172 1
  [4] Talmi I 1993 Simple Models of Complex Nuclei: The Shell Model and Interacting Boson Model (Harwood Academic)
  [5] Casten R F 1985 Phys. Lett. B 152 145
  [6] Kocheva D et al 2017 Eur. Phys. J. A 53 175
  [7] Karayonchev V et al 2021 Phys. Rev. C 103 044309
  [8] Stoyanova M et al 2019 Phys. Rev. C 100 064304
  [9] Kalaydjieva D et al 2021 Phys. Rev. C 104 024311
[10] Kocheva D et al 2020 Journal of Physics: Conf. Ser. 1555 012020
[11] Grahn T et al 2016 Eur. Phys. J. A 52 340
[12] Stone N J 2005 At. Data Nucl. Data Tables 90 75
[13] Alexander T K and Forster J S 1978 Adv. Nucl. Phys. 10 197
[14] Schwarzschild A Z and Warburton E K 1968 Ann. Rev. Nucl. Sci. 18 265
[15] Dewald A, Möller O and Petkov P 2012 Prog. Part. Nucl. Phys. 67 786
[16] Alexander T K and Bell A 1970 Nucl. Instrum. Methods 81 22
[17] Dewald A, Harissopulos S and von Brentano P 1989 Z. Phys. A 334 163
[18] Böhm G, Dewald A, Petkov P and von Brentano P 1993 Nucl. Inst. Meth. A 329 248
[19] Saha B 2004 Bestimmung der Lebensdauern kollektiver Kernanregungen in {}^{124}\!Xe \, und \, Entwicklung \, von \, entsprechender \, (2004) auch der Greichender (2004) a
         Analysesoftware PhD Thesis Universität zu Köln
[20] Astier A, Petkov P, Porquet M-G, Delion D S and Schuck P 2010 Phys. Rev. Lett. 104 042701
[21] Kondev F G 2008 Nucl. Data Sheets 109 1527
[22] Kocheva D et al 2017 Phys. Rev. C 96 044305
[23] Shimizu N, Mizusaki T, Utsuno T and Tsunoda Y 2019 Comput. Phys. Commun. 244 372
[24] Coraggio L et al 2012 Ann. Phys. (NY) 327 2125
[25] Machleidt R 2001 Phys. Rev. C 63 024001
[26] Bogner S, Kuo TTS, Coraggio L, Covello A and Itaco N 2002 Phys. Rev. C 65 051301(R)
[27] Chen J and Kondev F G 2015 Nucl. Data Sheets 126 373
[28] Kondev F G and Lalkovski S 2011 Nucl. Data Sheets 112 707
[29] Stoychev K et al 2023 Phys. Rev. C 108 014316
[30] Chiara C J and Kondev F G 2010 Nucl. Data Sheets 111 141
[31] Brown B A 2000 Phys. Rev. Lett. 85 5300
[32] Brown B A and Rae W D M 2014 Nucl. Data Sheets 120 115
[33] Towner I S 1987 Phys. Rep. 155 263-377
[34] Brown B A 1998 Phys. Rev. C 58 1
```